

RESEARCH

Open Access



Multi-omics reveals lactylation-driven regulatory mechanisms promoting tumor progression in oral squamous cell carcinoma

Fengyang Jing^{1,3}, Lijing Zhu^{1,3}, Jianyun Zhang^{1,3}, Xuan Zhou^{1,3}, Jiaying Bai¹, Xuefen Li², Heyu Zhang^{2,3*} and Tiejun Li^{1,3*}

*Correspondence:
zhangheyu1983@sina.cn;
litiejun22@vip.sina.com

¹ Department of Oral Pathology, Peking University School and Hospital of Stomatology, National Center of Stomatology, National Clinical Research Center for Oral Diseases, National Engineering Laboratory for Digital and Material Technology of Stomatology, Beijing Key Laboratory of Digital Stomatology, Research Center of Engineering and Technology for Computerized Dentistry Ministry of Health, NMPA Key Laboratory for Dental Materials, Beijing 100081, China

² Central Laboratory, Peking University School and Hospital of Stomatology, Beijing 100081, China

³ Research Unit of Precision Pathologic Diagnosis in Tumors of the Oral and Maxillofacial Regions, Chinese Academy of Medical Sciences (2019RU034), Beijing 100081, China

Abstract

Background: Lactylation, a post-translational modification, is increasingly recognized for its role in cancer progression. This study investigates its prevalence and impact in oral squamous cell carcinoma (OSCC).

Results: Immunohistochemical staining of 81 OSCC cases shows lactylation levels correlate with malignancy grading. Proteomic analyses of six OSCC tissue pairs reveal 2765 lactylation sites on 1033 proteins, highlighting its extensive presence. These modifications influence metabolic processes, molecular synthesis, and transport. CAL27 cells are subjected to cleavage under targets and tagmentation assay for accessible-chromatin with high-throughput sequencing, and transcriptomic sequencing pre- and post-lactate treatment, with 217 genes upregulated due to lactylation. Chromatin immunoprecipitation-quantitative PCR and real-time fluorescence quantitative PCR confirm the regulatory role of lactylation at the K146 site of dexh-box helicase 9 (DHX9), a key factor in OSCC progression. CCK8, colony formation, scratch healing, and Transwell assays demonstrate that lactylation mitigates the inhibitory effect of DHX9 on OSCC, thereby promoting its occurrence and development.

Conclusions: Lactylation actively modulates gene expression in OSCC, with significant effects on chromatin structure and cellular processes. This study provides a foundation for developing targeted therapies against OSCC, leveraging the role of lactylation in disease pathogenesis.

Keywords: Oral squamous cell carcinoma, Lactylation, Multi-omics analysis, Oncogenes

Oral squamous cell carcinoma (OSCC) is a malignancy that originating from squamous epithelial cells in the oral mucosa, accounting for approximately 90% of all global oral cancer cases [1–3]. The pathogenesis of OSCC is intricate, involving a nexus of genetic and environmental factors [4]. It is well-established that OSCC arises from a gradual malignant transformation of the oral mucosal squamous epithelium, culminating in



© The Author(s) 2024. **Open Access** This article is licensed under a Creative Commons Attribution-NonCommercial-NoDerivatives 4.0 International License, which permits any non-commercial use, sharing, distribution and reproduction in any medium or format, as long as you give appropriate credit to the original author(s) and the source, provide a link to the Creative Commons licence, and indicate if you modified the licensed material. You do not have permission under this licence to share adapted material derived from this article or parts of it. The images or other third party material in this article are included in the article's Creative Commons licence, unless indicated otherwise in a credit line to the material. If material is not included in the article's Creative Commons licence and your intended use is not permitted by statutory regulation or exceeds the permitted use, you will need to obtain permission directly from the copyright holder. To view a copy of this licence, visit <http://creativecommons.org/licenses/by-nc-nd/4.0/>.

cancer development. Oral leukoplakia (OLK) is the most prevalent potentially malignant lesion in the oral mucosa. However, the mechanisms driving the progression from OLK to OSCC remain poorly understood [5, 6]. Treatment strategies for OSCC include surgical resection, radiotherapy, and chemotherapy, with surgical resection as the primary intervention [7, 8]. Typically, a combined approach involving radiotherapy and chemotherapy accompanies surgery to mitigate recurrence and metastasis risks. Investigating protein expression patterns driving tumorigenesis in oral cancer is essential for devising effective preventive and therapeutic strategies. Such studies will enable personalized treatment decisions tailored to the individual patient conditions.

Beyond their impact on protein expression and subsequent effects on biological functions, post-translational modifications (PTMs) significantly influence protein stability, activity, and localization, crucially regulating protein function [9]. Common PTMs include acetylation, ubiquitination, methylation, phosphorylation, and glycosylation of amino acid residues [9–14]. Protein lysine lactylation (KLA), a novel PTM discovered in 2019, utilizes lactate as its substrate [15, 16]. Besides being the end product of glycolysis, lactate functions as a signaling molecule, suggesting novel roles of lactate through lactylation. This discovery provides fresh insights into the Warburg effect observed during tumor progression.

Since its identification, lactylation has been linked to various diseases, influencing the onset and progression of several cancers, including hepatocellular, gastric, non-small cell lung, colon, and breast cancers [17–21]. Lactylation may directly target histones and transcription factors, thereby affecting the transcription levels of key genes [22–24]. Moreover, lactylation has been detected on a wide range of proteins, including enzymes, signaling proteins, and secretory proteins, exerting extensive regulatory control over various cellular processes [25–28]. However, lactylation in oral cancer has not yet been reported.

This study conducted a comprehensive whole-proteome, high-throughput lactylome analysis to elucidate the lactylation profile associated with OSCC development. Utilizing an integrated approach combining cleavage under targets and tagmentation assay for accessible-chromatin with high-throughput sequencing, and RNA sequencing (CUT&TAG-seq, ATAC-seq, and RNA-seq), the potential regulatory network influenced by lactylation in OSCC progression was revealed. Our investigation also demonstrated that lactylation modification at the K146 site of dexh-box helicase 9 (DHX9) mitigates its inhibitory effects on OSCC (Supplemental Fig. 1), facilitating OSCC onset and progression. Furthermore, preliminary insights into the global regulatory role of lactylation, encompassing the modulation of oncogene expression and PTMs, were provided. These findings lay the groundwork for future scientific investigations and clinical applications.

Results

Alterations in global lactylation of proteins during OSCC progression

Immunohistochemical staining revealed a significant elevation in lactylation levels in OSCC tissues compared to normal adjacent tissues (NAT). A direct correlation was observed between the malignancy grade in OSCC and the extent of lactylation; as malignancy increased, lactylation levels also rose (Fig. 1a). Logistic regression analysis

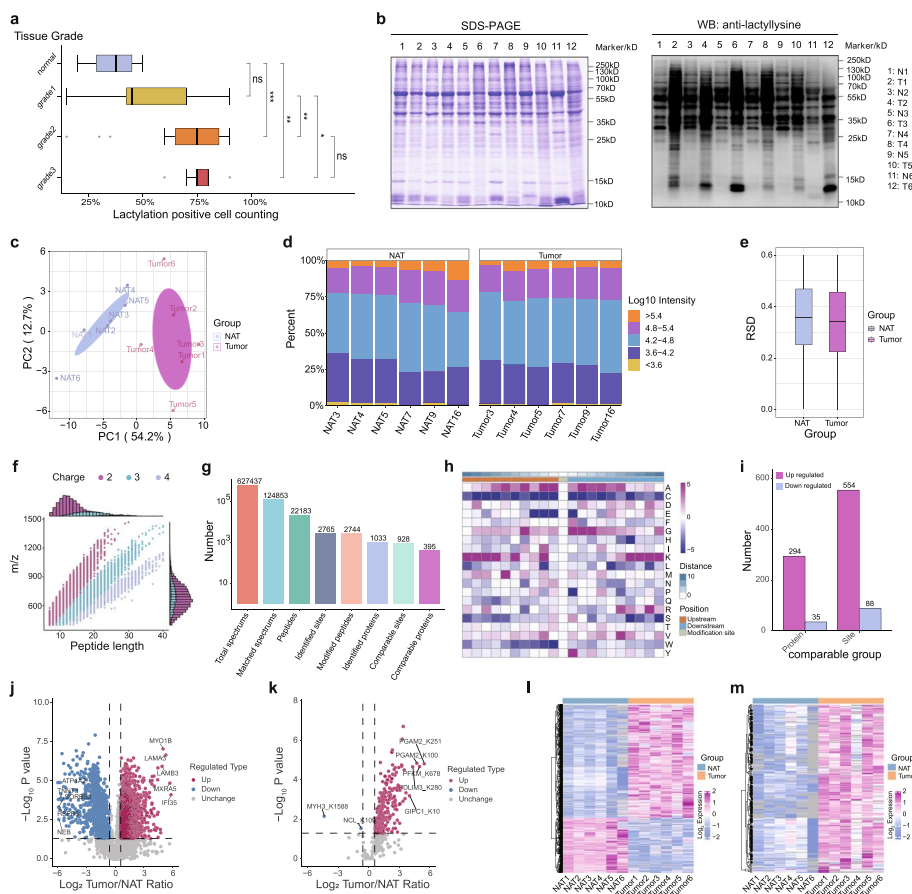


Fig. 1 In oral squamous cell carcinoma (OSCC), lacylation levels are significantly higher than in normal adjacent tissues (NAT). **a** The lacylation levels among varying OSCC grades (one-way ANOVA, ns: $P > 0.05$, $*P < 0.05$, $**P < 0.01$, $***P < 0.001$). **b** Western blot analysis determined lacylation levels in both OSCC and adjacent normal tissues. **c** Principal component analysis (PCA) was conducted using relative quantitative values, producing a visual PCA plot. **d** A sample distribution diagram illustrates intra- and inter-group data dispersion, with the horizontal axis representing sample names, and the vertical axis denoting percentages. Bar color indicates intensity values post- \log_{10} conversion. **e** A boxplot based on the relative standard deviation (RSD) of replicated samples' relative quantitative values within each group. **f** Quality control checks evaluated peptide length and charge distribution of digested protein samples. **g** Summary of identified lacylation sites and the total proteins filtered post-database retrieval. **h** Motif analysis of all identified lysine lacylation (KLA) proteins. **i** Bar charts display statistical data on differential proteins and modification sites after data processing and threshold selection. A volcano plot displaying differential proteins (**j**) and lacylation sites (**k**), with red dots indicating significant upregulation, blue dots indicating significant downregulation, and gray dots indicating no significant difference. A heatmap displaying the relative expression levels of multiple differential proteins (**l**) and lacylation sites (**m**) in different samples. Red represents high expression, blue indicates low expression, and gray denotes non-quantifiable values in the corresponding sample

was performed to exclude the influence of patient age and gender on the results (Additional file 1: Supplemental Fig. 2a). Detailed clinical information of the included patients is available in Additional file 2: Supplementary Table 1. Hematoxylin and eosin staining was used to determine the types of OSCC tissues and NAT, ensuring accurate tissue classification (Additional file 1: Supplemental Fig. 2b). Western blot analysis detected lacylation levels in OSCC tissues and NAT, revealing a significant increase in lacylation in tumor tissues (Fig. 1b). To identify proteins with significantly different lacylation levels between OSCC tissues and NAT, proteome and lacylome analyses were

performed. Sample quality assessment demonstrated distinct separation between various sample types (Fig. 1c), despite substantial heterogeneity in tumor tissues. A sample distribution chart indicated high sample quality (Fig. 1d). The relative standard deviation (RSD) based on quantification values for replicated samples within each group indicated consistent intragroup quantitative reproducibility (Fig. 1e). Enzymatic digestion of the samples followed by product detection revealed that most peptide fragments carried 2–3 charges, with peptide fragment lengths ranging from 7–20 amino acids, consistent with typical results in proteomic quality control (Fig. 1f). Comprehensive analysis elucidated 2765 lactylation sites on 1033 proteins, indicating widespread lactylation in OSCC (Fig. 1g). Examination of the motif features of these modified sites, analyzing peptide sequences (10 amino acids) upstream and downstream of all identified modified sites, revealed changes in the frequency of amino acids near the modified sites (Fig. 1h).

Identification of differential modification sites in OSCC

Differential analysis of all lactylation sites with valid quantitative data was conducted using the screening criterion of a P -value < 0.05 , with significant upregulation defined by a fold change exceeding 1.5 and significant downregulation by a fold change less than 1/1.5. A total of 642 lactylation sites on 329 proteins were identified, comprising 554 sites with increased lactylation and 88 sites with decreased lactylation (Fig. 1i). This finding aligns with expectations, given the Warburg effect in tumor tissues, leading to lactate accumulation compared to normal tissues. Differential analysis results of protein expression and lactylation levels were visualized as volcano plots (Fig. 1j, k; Additional file 1: Supplemental Fig. 3). And the corresponding quantitative data were presented as heatmaps (Fig. 1l, m), revealing both upregulation and downregulation of protein expression levels in OSCC compared to NAT, with a notable widespread upregulation of lactylation levels.

Impact of lactylation on biological functions and relevant signaling pathways in OSCC

Subcellular localization analysis of differentially modified proteins indicated that 44.2% of lactylation occurred in the cytoplasm and 28.57% in the nucleus (Additional file 1: Supplemental Fig. 4a). Functional classification enrichment analysis demonstrated that lactylation impacted various metabolic activities, including glycolysis, lipid metabolism, and amino acid metabolism, potentially influencing the transport of metabolites and signaling molecules (Additional file 1: Supplemental Fig. 4b). Subsequent Kyoto Encyclopedia of Genes and Genomes (KEGG) classification enrichment analysis revealed a significant impact of lactylation on cell growth and cellular communication. Among the diseases influenced by lactylation, inflammation-related diseases exhibited the highest susceptibility, followed by tumors. Additionally, associations were observed between lactylation and neurodegenerative diseases, cardiovascular diseases, metabolic diseases, and immune-related diseases (Additional file 1: Supplemental Fig. 4c). Previous studies have underscored the significant regulatory role of lactylation in these diseases.

To comprehensively elucidate the role of lactylation in OSCC, the molecular mechanisms governed by lactylation were investigated. Functional enrichment and pathway analyses of upregulated and downregulated datasets from proteomic and lactylation omic analyses were performed. Results indicated that proteomic functional enrichment

primarily encompassed gene expression and cellular functions, such as the negative regulation of gene expression, positive regulation of gene expression, cell migration, regulation of gene expression, positive regulation of gene expression, cell migration, regulation of biological processes, and regulation of cellular processes (Fig. 2a). Conversely,

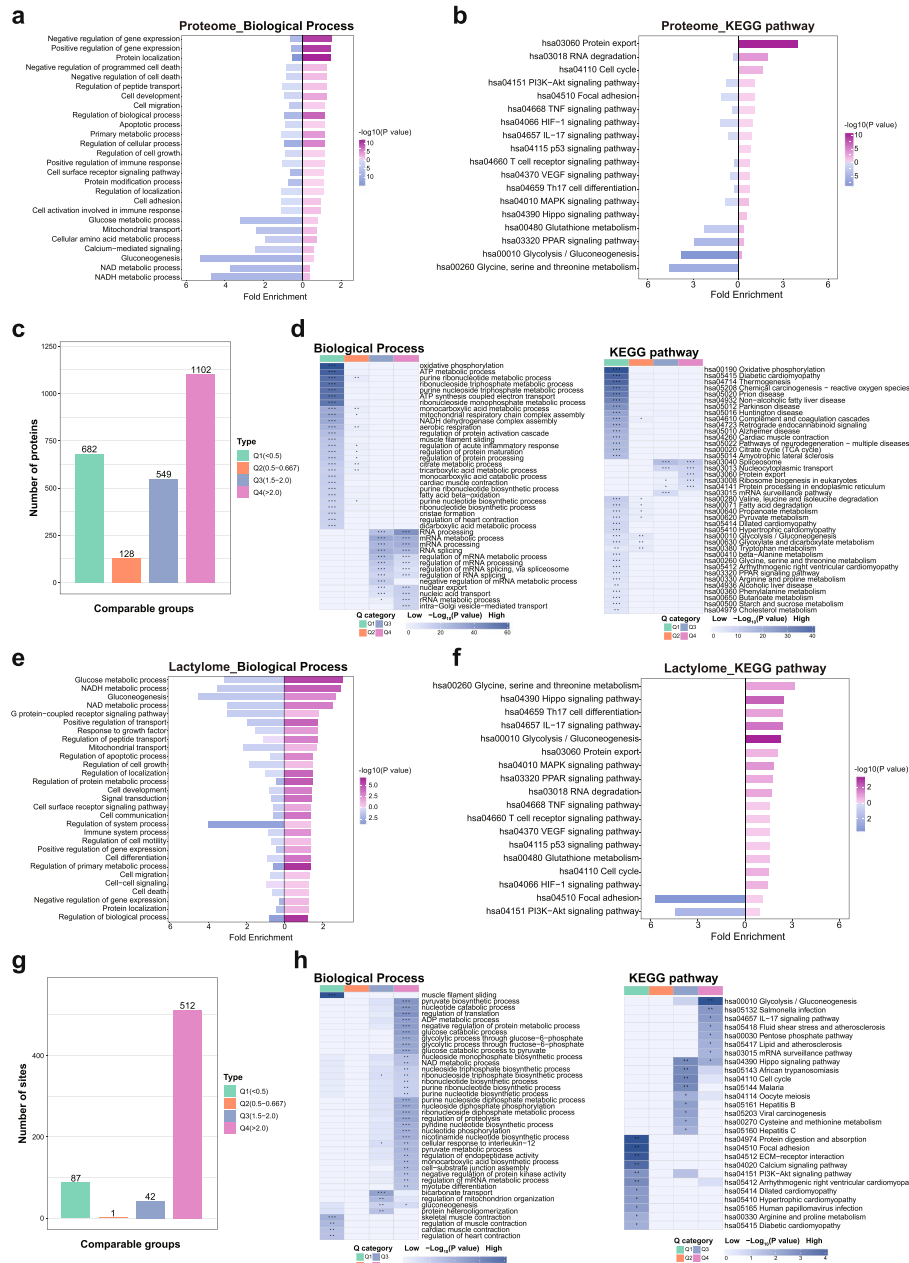


Fig. 2 Proteome and lactylome enrichment analysis. **a** Biological functional enrichment of differential proteins within the proteome. **b** Kyoto Encyclopedia of Genes and Genomes (KEGG) pathway enrichment of differential proteins in the proteome (one-way ANOVA, ns: $P > 0.05$, $*P < 0.05$, $**P < 0.01$, $***P < 0.001$). **c** Differentially expressed proteins were categorized into four groups based on fold change. **d** Biological functions and KEGG enrichment results of proteins exhibiting various fold changes. **e** Biological functional enrichment of differential proteins within the lactylome. **f** KEGG pathway enrichment of differential proteins in the lactylome. **g** Differentially expressed sites were classified into four groups according to fold change. **h** Biological functions and KEGG enrichment results of sites displaying different fold changes (one-way ANOVA, ns: $P > 0.05$, $*P < 0.05$, $**P < 0.01$, $***P < 0.001$)

lactylome enrichment predominantly included cellular metabolism, such as glucose metabolic processes, gluconeogenesis, and nicotinamide adenine dinucleotide (NAD⁺) metabolic processes. Additionally, lactylation significantly impacted signaling pathways and cellular activities, including the G protein-coupled receptor signaling pathway, signal transduction, cell surface receptor signaling pathway, regulation of cell growth, and cellular development (Fig. 2b). To determine the functional disparities among proteins with varying fold changes, these proteins were categorized into four groups based on their fold changes, denoted as Q1 to Q4 (Fig. 2c). Gene ontology (GO) and KEGG enrichment analyses were conducted for each group (Fig. 2d). Results revealed that, in addition to affecting metabolic activities, these proteins influenced mRNA activity, protein localization, signal transduction, and other processes.

In pathway enrichment, notable differences emerged between proteomics and lactylomics. Unlike the proteomic enrichment results, lactylation enrichment results showed elevated rankings for pathways such as glycine, serine, and threonine metabolism, the Hippo signaling pathway, T helper cell 17 (Th17) cell differentiation, the interleukin 17 (IL-17) signaling pathway, glycolysis/gluconeogenesis, and the mitogen-activated protein kinase (MAPK) signaling pathway. These pathways were predominantly concentrated in regions with heightened lactylation modifications (Fig. 2e, f). Concerning differential results, the proportion of high fold change Q4 in lactylation modification results exhibited a significantly greater magnitude compared to other groups (Fig. 2g). Enrichment analysis also underscored functions and pathways associated with tumors (Fig. 2h). This suggests that increased lactylation may play a pivotal regulatory role in these pathways during the occurrence and development of OSCC.

Lactylation-associated epigenetic regulation

To comprehensively elucidate the potential biological functions of lactylation in OSCC, its upstream regulatory role was investigated. Initially, the OSCC cell line CAL27 was exposed to 10 mM lactate for 24 h, resulting in increased lactylation levels post-treatment (Additional file 1: Supplemental Fig. 5a). Subsequently, both treated and control group samples underwent CUT&TAG-seq with a pan-anti-lactylation modification antibody, as well as ATAC-seq and RNA-seq analysis. This approach provided insights into lactylation-related epigenetic regulation, changes in chromatin accessibility, and alterations in gene expression under high lactate conditions.

Compared to the control group, CUT&TAG-seq and ATAC-seq results in the lactate treatment group showed peak aggregation of peaks near transcription start sites (TSS) suggesting that lactate enhances transcriptional processes (Additional file 1: Supplemental Fig. 5b). Separate differential analyses of CUT&TAG-seq and ATAC-seq data revealed that differentially identified peaks were primarily concentrated in promoter and distal intergenic regions, indicating significant lactylation impact on transcriptional regulation (Additional file 1: Supplemental Fig. 5c). Functional enrichment and KEGG pathway analyses of differential CUT&TAG-seq results provided further insights into functions and signaling pathways influenced by lactylation-associated histones. Enriched peaks, whether upregulated or downregulated post-lactate treatment, were predominantly linked to intracellular metabolic activities (Additional file 1: Supplemental Fig. 6a, b) and processes such as biosynthesis and gene expression. Pathway enrichment

analysis indicated that lactylation-associated histones significantly influenced not only metabolic-related signaling pathways but also the phosphatidylinositol-3-kinase/protein kinase B (PI3K/AKT), hypoxia-inducible factor-1 (HIF-1), and cancer-related signaling pathways (Additional file 1: Supplemental Fig. 6c, d).

To elucidate the genes associated with lactylation-related epigenetic regulation and chromatin accessibility, a comprehensive analysis integrating CUT&TAG-seq and ATAC-seq data from the untreated control group was conducted. Peaks located within a 3-kb range upstream and downstream of the TSS were defined as essential for gene transcription. Overlapping peaks between the three datasets were considered identical, and a Venn diagram visualized this overlap (Fig. 3a). The intersection revealed 14,518 peaks where lactylation positively correlated with chromatin accessibility. Peaks exclusively in the TSS and CUT&TAG-seq data but absent in the ATAC-seq data (2390 peaks) were regarded as negatively correlated with lactylation. Peaks near the TSS present only in ATAC-seq data totaled 18,164, indicating chromatin accessibility unrelated to lactylation, potentially influenced by other epigenetic mechanisms such as acetylation. These peaks were annotated with gene information. A similar joint analysis on lactate-treated samples revealed increased lactylation-driven chromatin accessibility, concomitant with the upregulation of other chromatin accessibility mechanisms (Fig. 3b). Analyzing CUT&TAG-seq and ATAC-seq data demonstrated that lactate treatment not only increased lactylation but also enhanced chromatin accessibility (Fig. 3c, Additional file 1: Supplemental Fig. 7a, b). Previous reports suggested that lactate treatment may also elevate acetylation levels, potentially contributing to increased chromatin accessibility.

Integrated multi-omics analysis: from epigenetics to transcription for identifying lactylation-driven oncogenes

To further investigate downstream functions governed by genes associated with lactylation and chromatin accessibility, we annotated the aforementioned positively and negatively correlated peaks to genes. Subsequently, ssGSEA was conducted based on the enrichment intensity of these genes in chromatin, allowing determination of their potential functions and relevant signaling pathways (Fig. 3d). Given the significantly higher number of positively correlated genes in CUT&TAG-seq and ATAC-seq compared to negatively correlated genes, and considering the likely predominant role of lactylation in promoting tumor progression in OSCC development, particular focus was placed on the mechanisms of oncogenes exhibiting increased chromatin accessibility driven by lactylation.

Enriched pathways of positively correlated genes exhibiting elevated scores in both CUT&TAG-seq and ATAC-seq samples were analyzed (Additional file 1: Supplemental Fig. 8). Lactylation-driven genes enriched in these pathways were retrieved and intersected with differential results from CUT&TAG-seq, ATAC-seq, and subsequent RNA-seq analyses. The results were visualized using an upset plot (Fig. 3e), revealing 217 lactylation-driven genes with increased expression, suggesting a potential oncogene set influenced by lactylation in OSCC.

Experimental validation of the aforementioned genes was performed. Chromatin immunoprecipitation-quantitative polymerase chain reaction (ChIP-qPCR) employing a pan-lactylation antibody was conducted on OSCC tissues and NAT to validate the

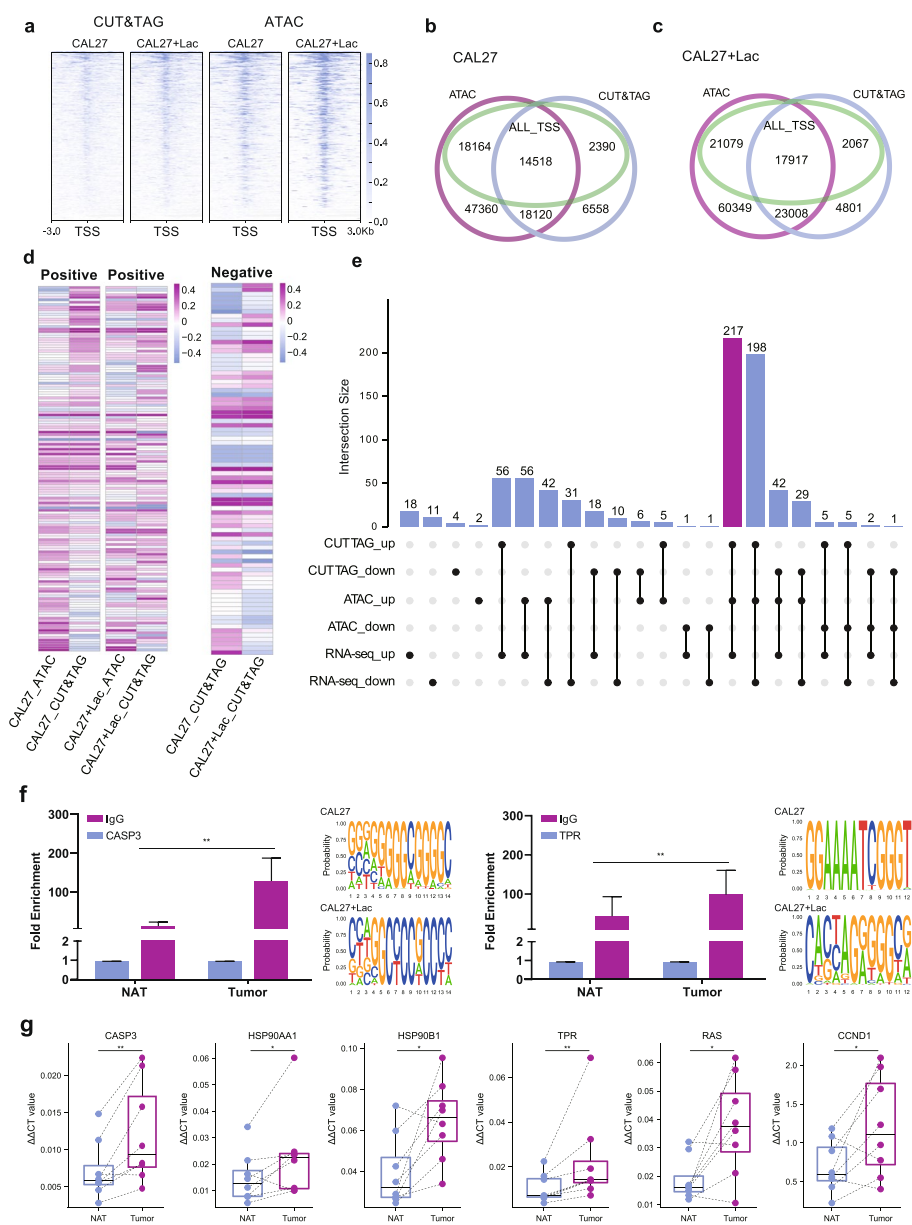


Fig. 3 Lactylation-driven expression of an oncogene set. **a** A heatmap depicts alterations in lactylation-associated gene expression and chromatin accessibility pre- and post-lactate treatment in the oral squamous cell carcinoma (OSCC) cell line CAL27. **b** Correlation analysis between lactylation-driven gene expression levels and chromatin accessibility. **c** Variations in lactylation-driven genes and chromatin accessibility in CAL27 cells exposed to high lactate concentrations. **d** Enrichment analysis of lactylation-driven genes and gene sets positively and negatively correlated with chromatin accessibility via single-sample gene set enrichment analysis (ssGSEA). **e** Intersection analysis of lactylation-driven gene sets positively correlated with chromatin accessibility and differentially expressed genes, determined by cleavage under targets and tagmentation sequencing (CUT&TAG-seq), assay for transposase-accessible chromatin with high-throughput sequencing (ATAC-seq), and RNA sequencing (RNA-seq). **f** Validation of increased lactylation enrichment in the promoter regions of *CASP3* and *TPR* in OSCC tissues through chromatin immunoprecipitation-quantitative polymerase chain reaction (ChIP-qPCR, two-tailed unpaired Student's *t*-test, $**P < 0.01$) and prediction of promoter sequences potentially affected by lactylation. **g** Validation of elevated expression of *CASP3*, *HSP90AA1*, *HSP90B1*, *TPR*, *RAS*, and *CCND1* in OSCC tissues through reverse transcription-quantitative polymerase chain reaction (RT-qPCR, two-tailed paired Student's *t*-test, $*P < 0.05$; $**P < 0.01$). Lac: lactate

transcriptional status of lactylation-driven genes (Fig. 3f). The results showed increased lactylation modifications proximal to the promoters of *CASP3* and *TPR* in tumor tissues compared to NAT samples, consistent with sequencing results. Concurrently, motif sequence information of lactylation-driven gene expression was predicted. RNA extracted from OSCC tissues and paired NAT underwent RT-qPCR to validate transcriptional alterations of select potential oncogenes (Fig. 3g). The results demonstrated significant upregulation of *CASP3*, *HSP90AA1*, *HSP90B1*, *TPR*, *RAS*, and *CCND1* in OSCC relative to NAT, aligning with previous analyses. This suggests these key genes may be influenced by lactylation, contributing to their upregulated expression.

DHX9-146K1a potentially reverses the inhibitory impact of DHX9 on OSCC

The identified 217 lactylation-driven potential oncogenes, which exhibit upregulated expression during oral cancer carcinogenesis, may be linked to chromatin structure openness, indicating a pivotal role for chromatin helicases in the progression of oral cancer. During the carcinogenesis of oral cancer, specific helicases likely facilitate chromatin opening, thereby enhancing the expression of numerous genes.

In previous work [29], a diagnostic model for oral cancer carcinogenesis was developed, with *DHX9* identified as a critical component. *DHX9*, a multifunctional nuclear protein, is significantly involved in RNA processing, transcription, and translation. Protein–protein interaction network analysis of *DHX9* and oncogenes revealed direct interactions with proteins such as *HIF-1A*, *TPR*, *MDM2*, and *BRCA1*, with downstream molecules including *CASP3*, *KRAS*, *MAPK1*, *HSP90AA1*, and *PIK3CA* (Additional file 1: Supplemental Fig. 9a). Sequencing results indicated a marked increase in the lactylation level of *DHX9* in OSCC compared to NAT (Additional file 1: Supplemental Fig. 9b). Further examination of *DHX9*'s protein structure identified a potential lactylation modification site at lysine 146 (Fig. 4a).

Overexpression of *DHX9* in LEUK1 (Oral Leukoplakia Cell Line) and CAL27 (Oral Adenosquamous Carcinoma Cell Line) cells validated via reverse transcription-quantitative polymerase chain reaction (RT-qPCR) and western blot analysis (Fig. 4b, c). Cell proliferation, assessed through a cell counting kit-8 (CCK8) assay, showed significant inhibition with *DHX9* overexpression in both cell types, corroborated by clone formation assays (Fig. 4d, e). The impact of overexpressed *DHX9* on cell migration and invasion was analyzed using scratch healing and Transwell assays (Fig. 4f, g), revealing that *DHX9* effectively suppresses these capabilities. To validate these conclusions, *DHX9* was knocked down using two distinct vectors in LEUK1 and CAL27 cells, confirming knockdown efficiency (Fig. 4h, i). Subsequent CCK8 and clone formation assays demonstrated a significant increase in cell proliferation following *DHX9* knockdown (Fig. 4j, k), while scratch healing (Fig. 4l) and Transwell assays (Fig. 4m) showed enhanced cell migration and invasion. These results suggest that *DHX9* exerts an inhibitory effect on the occurrence and progression of OSCC.

Proteomic lactylation sequencing data identified lactylation at 146 lysine residues of *DHX9*. To investigate the functional impact of *DHX9* lactylation, we introduced the K146R (arginine) mutation, to inhibit lactylation and the K146T (threonine) mutation to mimic lactylation. Using lentivirus, LEUK1 and CAL27 cells were separately infected with control plasmids, wild-type overexpression plasmids, and two mutation plasmids.

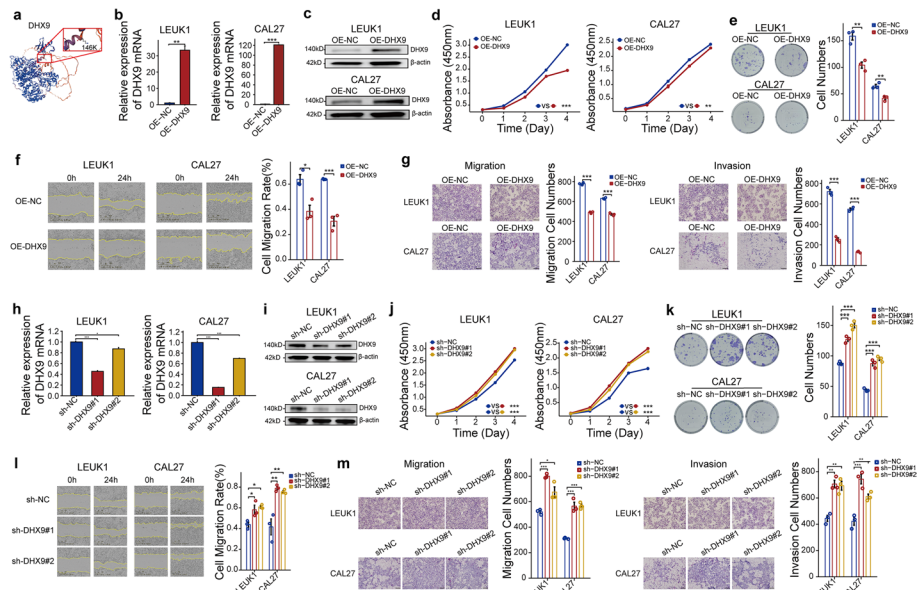
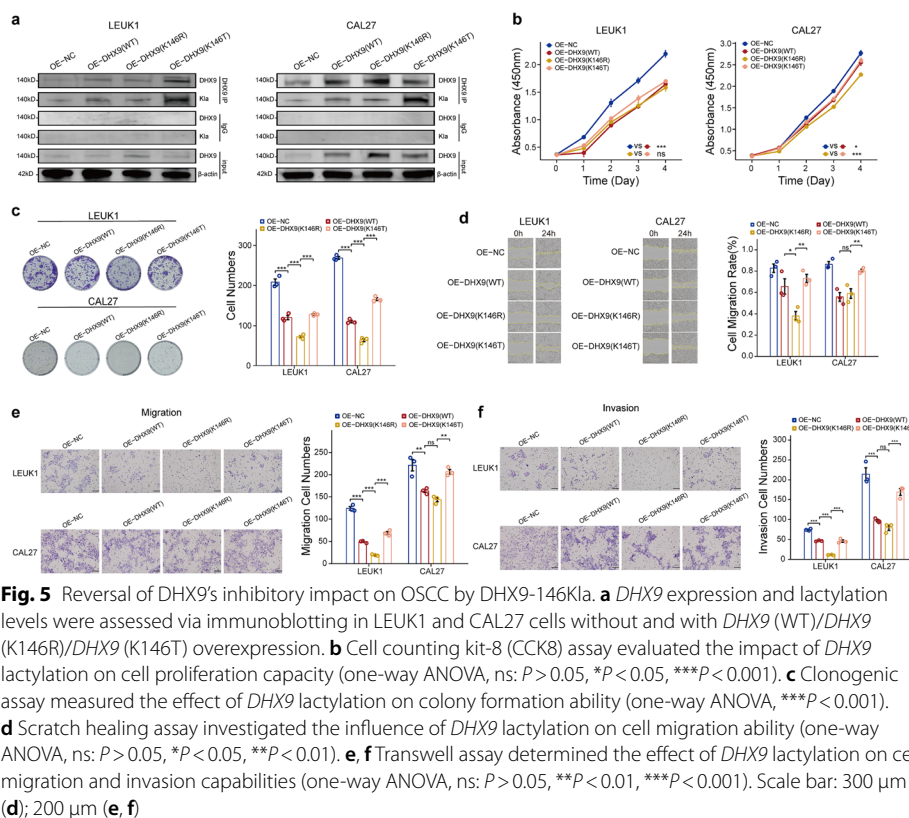


Fig. 4 Suppression of OSCC onset and progression by DHX9. **a** The protein structure of *DHX9* and the potential lactylation modification site. Reverse transcription-quantitative polymerase chain reaction (RT-qPCR) (**b**) and western blot (**c**) analysis of the expression of *DHX9* overexpression in LEUK1 and CAL27 cells (two-tailed unpaired Student's *t*-test, ***P* < 0.01, ****P* < 0.001). **d** Cell counting kit-8 (CCK8) assay to evaluate changes in cell proliferation capacity (one-way ANOVA, ***P* < 0.01, ****P* < 0.001). **e** Clonogenic assay to assess alterations in colony formation ability (two-tailed unpaired Student's *t*-test, ***P* < 0.01). **f** Scratch healing assay to examine changes in cell migration ability (two-tailed unpaired Student's *t*-test, **P* < 0.05, ****P* < 0.001). **g** Transwell assay to investigate changes in cell migration and invasion capabilities (two-tailed unpaired Student's *t*-test, ****P* < 0.001). RT-qPCR (**h**) and western blot (**i**) analysis of the expression of downregulated *DHX9* in LEUK1 and CAL27 cells (one-way ANOVA, **P* < 0.05, ****P* < 0.001). **j** CCK8 assay to evaluate changes in cell proliferation (one-way ANOVA, ****P* < 0.001). **k** Clonogenic assay to assess alterations in colony formation ability (one-way ANOVA, ****P* < 0.001). **l** Scratch healing assay to examine changes in cell migration ability (one-way ANOVA, **P* < 0.05, ***P* < 0.01). **m** Transwell assay to measure modifications in cell migration and invasion capabilities (one-way ANOVA, **P* < 0.05, ***P* < 0.01, ****P* < 0.001). Scale bar: 300 μm (**f**, **l**); 200 μm (**g**, **m**)

Co-IP and western blot analyses confirmed reduced lactylation levels in the K146R mutant and elevated levels in the K146T mutant (Fig. 5a). A CCK8 assay revealed that both wild-type and mutant *DHX9* inhibited cell growth compared to the control group, with the K146T mutant showing weaker inhibition than the K146R mutant, particularly in the CAL27 OSCC cell line (Fig. 5b). These results suggest that lactylated *DHX9* may significantly promote OSCC occurrence. Cloning experiments further demonstrated that inhibiting *DHX9* lactylation strongly inhibits cell proliferation, whereas simulating lactylation mutations reversed this effect (Fig. 5c). Finally, scratch healing and Transwell assays showed that blocking *DHX9* lactylation during overexpression significantly inhibited cell migration and invasion, while simulating lactylation reversed this inhibition (Fig. 5d–f). We also conducted a qPCR assay to evaluate the expression levels of *CASP3*, *RAS*, *MAPK1*, *HSP90AA1*, and *PIK3CA* in the CAL27 cell line (Additional file 1: Supplementary Fig. 9c). The results revealed a notable downregulation of these genes in cells overexpressing the *DHX9* lactylation-inhibiting vector (K146R mutant). Conversely, a pronounced upregulation of gene expression was observed in cells harboring the lactylation vector (K146T mutant). These findings further confirm the crucial role of *DHX9* lactylation in regulating the expression of these oncogenes within oral cancer cells.



Discussion

OSCC, the predominant form of oral cancer, follows a complex multi-stage progression and shows a correlation with potentially malignant oral mucosal diseases [29–31]. Metabolic pathway dysregulation is a hallmark of cancer development [32, 33]. In OSCC, tumor cells predominantly use aerobic glycolysis for ATP production [34–36], necessitating a substantial glucose supply to sustain rapid growth and proliferation [37, 38]. While regulatory mechanisms are not fully elucidated, the association between OSCC development and alterations in various biological processes and molecular functions is undeniable [39, 40]. A deeper understanding of the metabolic characteristics and epigenetic status of OSCC tumors could provide valuable insights into OSCC mechanisms and potential therapeutic interventions.

Our integrated analysis provided significant insights into lactylation's regulatory mechanisms in OSCC. Lactylation was found to induce caspase3 expression in OSCC cells, leading to its significant upregulation. Research indicates that caspase3, aside from its pivotal apoptotic role, also promotes tumor development and metastasis [41]. Although specific mechanisms remain unclear, caspase3's procancer function is linked to double-stranded DNA breakage. Lactylation of the caspase3 protein itself may contribute to its procancer function; however, this molecular mechanism requires further exploration. Additionally, lactylation was found to drive TPR expression. TPR, predominantly localized in the nucleus, can activate the Ras protein [42], influencing downstream signaling pathways like PI3K/AKT and MAPK, relevant to

tumor development. TPR's susceptibility to lactylation might be linked to its role in Ras protein activation.

This study revealed a significant interaction between *DHX9* and multiple oncogenes. *DHX9*, a multifunctional RNA/DNA helicase, plays a complex role in cancer occurrence and development [43]. It is involved in DNA replication, transcription, and RNA processing, and its abnormal expression can lead to DNA damage and genomic instability [44–47]. *DHX9* influences the accumulation of endogenous nucleic acids (typically dsRNA), activating the innate immune response in cancer cells, thus enhancing tumor response to immune checkpoint inhibitor therapy [47–49]. *DHX9* can also alter immune cell infiltration in the tumor microenvironment, affecting cancer progression [49]. Notably, *DHX9* is susceptible to lactylation. Our observations in OLK and OSCC cells demonstrated that *DHX9* inhibits cell proliferation, migration, and invasion, acting as a protective factor against tumorigenesis. However, this protective effect is reversed when *DHX9* undergoes lactylation, promoting OSCC development. Understanding these intricate molecular mechanisms not only enhances our grasp of OSCC but also suggests potential targeted therapeutic strategies. This underscores the critical role of lactylation in OSCC regulatory processes, offering promising avenues for innovative therapies.

Metabolic diseases, followed by tumors, are the primary diseases involved in lactylation regulation. Key cellular functions include various metabolic processes, such as glucose, lipid, and amino acid metabolism, as well as intracellular signal transduction, cell division, cell structure, and molecular transport. Additionally, enrichment in classical pathways like the HIF-1, PI3K/AKT, and Hippo signaling pathways in OSCC was observed. These pathways play key regulatory roles in tumor development [50–55]. *DHX9*'s role within these signaling cascades is intricate and multi-dimensional. It is posited that *DHX9* modulates the transcriptional activity of pivotal players within the HIF-1 α , PI3K, PDK1, YAP, and TAZ pathways, either by regulating their expression or engaging in direct molecular interactions. This modulation could, in turn, alter the abundance of these signaling molecules and the cascade of downstream events they initiate [56–61]. However, their influence on lactylation in OSCC remains unexplored. Acting as a central node, *DHX9* might orchestrate a convergence of signals from these pathways, thereby propelling the transcriptional machinery that underpins the malignant traits of OSCC. These results align with current tumor biology knowledge and provide novel avenues for OSCC prevention and treatment strategies.

Despite offering a thorough understanding of lactylation's regulatory role in OSCC, a limitation of this correlation analysis is its predominant reliance on OSCC cell lines. This choice stems from the greater stability of molecular regulatory mechanisms in cell lines compared to the substantial heterogeneity observed in tumor tissues, which complicates the identification of consistent driver genes. The enrichment of lactylation in tissues and the validation of gene expression levels substantiate the credibility of these results to some extent. Future research should include an analysis of lactylation in additional OSCC tissue specimens to enhance understanding of lactylation's regulatory function in driving tumor development.

In summary, this study presents comprehensive regulatory characteristics of lactylation in OSCC, integrating lactylation-associated chromatin accessibility-driven gene transcription and post-translational lactylation. Furthermore, it elucidates the role and

potential molecular mechanisms of lactylation in OSCC progression, outlining a regulatory network. These findings offer a valuable new perspective for exploring OSCC's biological functions and may enhance understanding of the disease's occurrence and progression. Consequently, this knowledge could contribute to the development of improved clinical management strategies and treatment approaches.

Conclusions

In conclusion, this study reveals the significant role of lactylation in the progression of OSCC, particularly in regulating signal pathways and gene expression associated with tumor development. The study particularly focuses on the DHX9 protein, finding that lactylation of DHX9 may play a key role in the occurrence and development of OSCC. The results provide potential targets for the development of new therapeutic strategies against OSCC.

Methods

Sample collection

An initial cohort comprised 109 samples from 95 patients, including 14 matched pairs. Among the paraffin-embedded samples, there were 8 NAT and 73 OSCC tissues, while the frozen samples consisted of 14 OSCC and 14 NAT tissues. All specimens were sourced from the Biobank of Peking University School and Hospital of Stomatology. Immunohistochemical staining was performed on all paraffin samples, and proteomic and lactylomic analyses were conducted on six pairs of tissue samples. Additionally, eight additional tissue samples were used for experimental validation.

Immunohistochemistry

Serial 4- μ m thick tissue sections were stained using the Chem Mate Envision system (K5007, Dako). Antigen retrieval was conducted with 1 mM ethylene diamine tetraacetic acid (EDTA). The sections were then incubated with a pan anti-lactyllysine antibody (PTM-1401RM, PTM-Bio) at a 1:100 dilution. Immunocomplexes were visualized using the 3,3'-Diaminobenzidine Liquid Plus Substrate Plus Chromogen System (Dako, Glostrup, Denmark) and counterstained with hematoxylin for light microscopy examination. Two pathologists independently evaluated the immunostaining results, blinded to patient information.

Protein extraction

Tissues stored at -80°C were placed on ice, cut into 1 mm^3 pieces using sterile scissors, and added to a 1% Triton buffer in a 4:1 ratio containing $1\times$ protease inhibitor cocktail and $1\times$ phenylmethanesulfonyl fluoride. The tissues were homogenized, incubated on ice for 30 min, sonicated, and centrifuged at 12,000 g for 10 min at 4°C . For cell samples, the medium was discarded, cells were washed twice with phosphate-buffered saline (PBS), lysed in an appropriate amount of lysis buffer with $1\times$ protease inhibitor cocktail, and incubated on ice for 30 min. Cells were then transferred to a centrifuge tube and centrifuged at 12,000 g for 10 min at 4°C . The resulting supernatant was the tissue protein extract, and its protein concentration was determined using a bicinchoninic acid assay kit (P0010, Beyotime). The extract was stored at -80°C for future experiments.

Trypsin digestion

Equal amounts of each protein sample were enzymatically digested [62]. The volume was adjusted to match that of the lysis buffer, followed by the gradual addition of 20% trichloroacetic acid and thorough vortexing. The mixture was precipitated at 4 °C for 2 h, centrifuged at 4500 g for 5 min, and the supernatant discarded. The precipitate underwent two to three washes with pre-cooled acetone. After air-drying, 200 mM triethylammonium bicarbonate was added, and the mixture was sonicated to disperse the precipitate. Trypsin was introduced at a 1:50 (enzyme to protein) ratio for overnight digestion. Dithiothreitol was then added to a final concentration of 5 mM, and the mixture was reduced at 56 °C for 30 min. Iodoacetamide was subsequently added to a final concentration of 11 mM, and the mixture was incubated at 25 °C in the dark for 15 min.

Liquid chromatography-mass spectrometry (LC-MS) analysis

Peptide segments were dissolved in mobile phase A of liquid chromatography and separated using the Easy-nLC1000 Ultra-High-Performance Liquid Chromatography System. Mobile phase A comprised an aqueous solution containing 0.1% formic acid and 2% acetonitrile, while mobile phase B consisted of acetonitrile–water with 0.1% formic acid. The liquid phase gradient was programmed as follows: 0–70 min, transitioning from 9 to 25% B; 70–82 min, from 25 to 35% B; 82–86 min, from 35 to 90% B; and 86–90 min, at 90% B, maintaining a flow rate of 450 nL/min. Following separation using the ultra-high-performance liquid chromatography system, the peptide segments were ionized through the capillary ion source for ionization and subsequently analyzed with the TimsTOF Pro mass spectrometer.

Modification enrichment

Peptide segments were dissolved in an immunoprecipitation buffer (containing 100 mM NaCl, 1 mM EDTA, 50 mM Tris–HCl, 0.5% NP-40, pH 8.0). The supernatant was transferred to pre-washed resin (PTM1404, PTM-Bio) and placed on a rotating shaker at 4 °C for gentle overnight incubation. The resin was then sequentially washed four times with IP buffer and twice with deionized water. Peptides bound to the resin were eluted with 0.1% trifluoroacetic acid solution, with three elutions performed. The eluate was collected and subjected to vacuum freeze-drying. After drying, desalting was performed following the C18 ZipTips instructions. A final round of vacuum freeze-drying was done, and the samples were prepared for LC–MS analysis.

Database search

Secondary mass spectrometry data was analyzed using MaxQuant [63] (v1.6.15.0). The database utilized was Homo_sapiens_9606_SP_20230103.fasta, containing 20,389 sequences. To assess the false discovery rate from random matches, a decoy database was employed. Additionally, a common contaminant database was included to mitigate the impact of contaminating proteins on the identification results. The mass

tolerance for first-level precursor ions for both the initial and primary searches was set at 20 ppm, as was the mass tolerance for second-level fragment ions.

ATAC-seq

Nuclei were extracted from the samples, and the nuclei pellet was reconstituted using a Tn5 transposase reaction mixture. Equimolar amounts of Adapter 1 and Adapter 2 were added post-transposition, followed by PCR amplification of the library. The Illumina Novaseq platform was then utilized for library sequencing, producing 150-bp paired-end reads [64].

CUT&TAG-seq

Cells were immobilized onto Concanavalin A-coated magnetic beads, and digitonin was used to permeabilize the cellular membrane. The pA-Tn5 transposase enzyme, guided by a corresponding antibody, precisely bound to the DNA sequence near the target protein, resulting in factor-specific tagmentation. An anti-pan-lactyllysine antibody (PTM-Bio, PTM-1401RM) was used in this experiment. DNA sequences were tagmented, with adapters affixed to both ends. These tagged sequences were then amplified through PCR to generate sequencing-ready libraries. The libraries were purified using AMPure beads, and library quality was assessed using the Agilent Bioanalyzer 2100 System [65].

RNA-seq

Total RNA served as the starting material for RNA sample preparations. In brief, mRNA was isolated from the total RNA using magnetic beads conjugated to poly-T oligonucleotides. Complementary DNA (cDNA) products were generated via reverse transcription. PCR was performed using Phusion High-Fidelity DNA polymerase, universal PCR primers, and Index Primer. Finally, PCR products were purified using the AMPure XP System, and library quality was assessed using the Agilent Bioanalyzer 2100 System. The raw data in fastq format (raw reads) underwent preprocessing using custom Perl scripts.

Single sample gene set enrichment analysis (ssGSEA)

To elucidate the biological roles of gene sets influenced by lactylation-driven expression and chromatin accessibility, ssGSEA was performed [66]. This method computes a score for each sample by correlating it with the relevant gene set, converting the gene expression profile into an enrichment profile. This transformation allows for the evaluation of the significance of various functional signaling pathways. For this analysis, the “c2.cp.kegg.v6.2.-symbols” gene set was sourced from the MSigDB database [67].

Chromatin immunoprecipitation (ChIP)

Tissue samples were weighed, with each ChIP experiment utilizing 25 mg of tissue. The samples were kept at a low temperature to prevent protein degradation and finely minced with sterile scissors. After rinsing with PBS, formaldehyde was added to a final concentration of 1%, followed by a 10-min incubation at 37 °C. ChIP sequencing (ChIP-seq) was conducted using a ChIP-seq kit (9005S, Cell Signaling Technology) according to the provided protocol. An antibody against pan-lactyllysine (PTM-Bio, PTM-1401 RM) was employed in the experiment. Finally, DNA was purified using a DNA purification kit

and analyzed via quantitative PCR (qPCR) using specific primers. Detailed primer information for ChIP-qPCR is provided in Additional file 2: Supplemental Table 2.

Real-time fluorescence qPCR (RT-qPCR)

Tissues were maintained at low temperatures and finely minced. RNA was extracted and purified using the RNA-Quick Purification Kit (RN001, ESscience) following the manufacturer's guidelines. The RNA was then reverse transcribed into cDNA using the RT Reagent Kit with a gDNA Eraser (RR047A, Takara). qRT-PCR was performed using the Bio-Rad CFX96 Real-Time PCR Detection System with SYBR Green PCR Master Mix (A25741, Thermo Fisher Scientific). Primer sequences for qRT-PCR are listed in Additional file 2: Supplemental Table 3.

Cell culture

The OLK cell line LEUK1, the OSCC cell line CAL27, and HEK293T cells were obtained from the laboratory of Peking University School and Hospital of Stomatology. LEUK1 cells were cultured in 1640 medium, while CAL27 and HEK293T cells were cultured in Dulbecco's Modified Eagle Medium (DMEM). All cells were supplemented with 10% fetal bovine serum and incubated at 37 °C in a cell culture incubator with 5% carbon dioxide. In the treatment group, cells were exposed to 10 mM lactate for 24 h. The cell lines used have all been authenticated and are free from mycoplasma contamination.

Lentiviral transduction and transfection

Gene knockout experiments were conducted using short hairpin RNAs (shRNAs) delivered via lentiviral transduction. The PLKO.1 plasmid, containing the shRNA-*DHX9* targeting sequence, was co-transfected with psPAX2 and PMD2.G plasmids in a 2:2:1 ratio into HEK293T cells, producing the shRNA-*DHX9* lentivirus. Concurrently, co-transfection of pCDH-*DHX9*-WT/K146R/K146T, psPAX2, and PMD2.G plasmids (in a 2:2:1 ratio) into HEK293T cells generated a lentivirus overexpressing *DHX9*-WT/K146R/K146T genes. Post-transfection, cell supernatant containing lentiviral particles was collected, filtered through a 0.45- μ m filter, and used to infect target cells. Polybrene was added at 8 μ g/mL, followed by selection with 5 μ g/mL puromycin to identify stable transfectants. The shRNA target sequences employed are detailed in Additional file 2: Supplemental Table 4.

Co-immunoprecipitation (co-IP)

Cell lysates were prepared using a lysis buffer consisting of 150 mM sodium chloride, 20 mM HEPES (pH 7.4), 2 mM EDTA, 1.5 mM magnesium chloride, and 0.5% NP-40. A protease inhibitor cocktail was added to the lysates, and co-immunoprecipitation (co-IP) was performed using an anti-*DHX9* antibody (ab26271, Abcam). The immunocomplexes were incubated with protein A/G-sepharose (Invitrogen) at 4 °C for 6 h, followed by six washes with IP buffer, and eluted at 95 °C for 15 min. The eluted protein samples were then subjected to western blot analysis.

Western blot

Protein samples were combined in a 4:1 ratio with 5 × loading buffer for sodium dodecyl sulfate–polyacrylamide gel electrophoresis (SDS-PAGE) and heated at 95 °C for 10 min. The proteins were separated via SDS-PAGE, transferred onto a nitrocellulose filter membrane, and blocked with non-fat milk. The membrane was probed with primary antibodies (anti-DHX9, ab26271, Abcam, diluted 1:1000; pan-anti-lactyllysine, PTM-1401RM, PTM-Bio, diluted 1:1000; anti-β-actin, 81115–1-RR, Proteintech, diluted 1:5000) overnight. Following rinsing, the blots were incubated with secondary antibodies and finally exposed.

Cell counting kit-8 (CCK8)

Cell proliferation was quantified using a CCK8 assay kit (CK001, Lablead). Cells were seeded in 96-well plates at a density of 4×10^3 cells per well, with 100 μL of complete culture medium added to each well. At specified intervals, the medium was replaced with 100 μL of DMEM containing 10 μL of CCK8 dye. Optical density at 450 nm was measured using a microplate reader (Biotec). This experiment was performed in triplicate, with statistical analysis and visualization conducted using R package software (version 4.0.2).

Cloning formation assay

Cells from various groups were seeded in six-well plates at a density of 1×10^3 cells per well and incubated for 2 weeks. Subsequently, the culture medium was discarded, and cells were fixed with 4% paraformaldehyde for 10 min, followed by staining with 0.5% crystal violet. Each experiment was independently replicated three times. The results were analyzed using ImageJ software, and quantitative data were further subjected to statistical analysis and visualization with R package software (version 4.0.2).

Wound healing assay

Cells designated for testing were seeded in 96-well plates and cultured to form a confluent monolayer. Following pre-treatment with serum-free medium for 12 h, a straight-line scratch was created in the cell monolayer using a sterile pipette tip. Cells were washed twice with PBS to remove debris and then incubated in a serum-free medium. Cell migration was monitored at 0, 12, and 24 h under an inverted microscope, with images captured at each time point. The cell migration rate (%) was calculated using the formula: (wound distance at 0 h – wound distance at 12 h/24 h)/wound distance at 0 h. The experiment was recorded and analyzed using the IncuCyte ZOOM system from Essen BioScience.

Transwell assay

In invasion experiments, 6 μL of matrix gel combined with 54 μL of serum-free culture medium was pre-incubated in a chamber at 37 °C for 6 h. The tested cells were suspended in a serum-free culture medium and introduced into the chambers (5×10^4 cells per well). The lower chamber was supplemented with a medium containing 10% serum. After 48 h of incubation, cells on the upper surface were removed with

a cotton swab, while those on the lower surface were fixed with 4% paraformaldehyde, stained with Giemsa, and quantified under a microscope to assess the number of cells that traversed the membrane. Each experiment was conducted independently in triplicate. Quantitative data obtained from the experimental results were analyzed using ImageJ software, followed by statistical analysis and visualization with R software (version 4.0.2).

Statistical analysis

Calculations and statistical analyses were executed with the R software package (v4.0.2). Continuous variables were compared using either the two-tailed unpaired Student's *t*-test or the two-tailed paired Student's *t*-test with a significance threshold of $P < 0.05$, unless otherwise stated.

Supplementary Information

The online version contains supplementary material available at <https://doi.org/10.1186/s13059-024-03383-8>.

Additional file 1: Fig. S1. Schematic illustration of multi-omics analysis and experimental validation in this study. Fig. S2. Clinical information of patients with oral squamous cell carcinoma (OSCC). Fig. S3. Differential proteins and lactylation sites in OSCC tissues and NAT. Fig. S4. Functional/pathway classification analysis of differentially lactylated proteins. Fig. S5. Genomic alterations in OSCC cells following lactate treatment. Fig. S6. Functional/pathway enrichment analysis of peaks influenced by lactylation-associated chromatin-binding proteins. Fig. S7. Impact of lactate on chromatin accessibility and lactylation-associated gene expression in OSCC cells. Fig. S8. Functional pathways enriched by genes positively correlated with epigenetic regulation associated with lactylation modification and chromatin accessibility. Fig. S9. DHX9 plays a crucial role in the development of OSCC.

Additional file 2: Table S1. Clinical characteristics data. Table S2. The ChIP-qPCR assay primers. Table S3. The quantitative real-time PCR primers. Table S4. The shRNA target sequences.

Additional file 3. Uncropped blot images.

Additional file 4. Review history.

Acknowledgements

The authors express their gratitude to Jingjie PTM BioLab Incorporated Company (Hangzhou) for their assistance with quantitative proteomic and lactylomic analysis.

Peer review information

Wenjing She was the primary editor of this article and managed its editorial process and peer review in collaboration with the rest of the editorial team.

Review history

The review history is available as Additional file 4.

Authors' contributions

HZ and TL conceived and designed the study. FJ, LZ, and JZ conducted data acquisition for cell line studies. FJ, XZ, JB, and XL provided administrative, technical, and material support. FJ, LZ, JZ, and XZ were involved in the analysis and interpretation of data. FJ, LZ, JZ, XZ, HZ, and TL were responsible for drafting and revising the manuscript. HZ and TL supervised the study. FJ, JZ, HZ, and TL had access to and verified all of the data in the study.

Funding

This work was supported by research grants from the National Nature Science Foundation of China [grant number 81671006, 81300894], the CAMS Innovation Fund for Medical Sciences [grant number 2019-I2M-5-038], and National clinical key discipline construction project [grant number PKUSSNKP-202102].

Availability of data and materials

The mass spectrometry proteomics data have been deposited to the ProteomeXchange Consortium via the PRIDE [68] partner repository with the dataset identifier PXD047535 [69] and PXD047673 [70]. The CUT&TAG-seq, ATAC-seq, and RNA-seq data have been uploaded to the GEO database with the accession number GSE249223 [71], GSE249224 [72], and GSE249226 [73], respectively. No other scripts and software were used other than those mentioned in the "Methods" section.

Declarations

Ethics approval and consent to participate

The study protocol received approval from the Ethics Committee of Peking University School and Hospital of Stomatology (Number: PKUSSIRB-202385026).

Consent for publication

Not applicable.

Competing interests

The authors declare that they have no competing interests.

Received: 5 March 2024 Accepted: 30 August 2024

Published online: 15 October 2024

References

- Leusink FK, van Es RJ, de Bree R, Baatenburg de Jong RJ, van Hooff SR, Holstege FC, Slootweg PJ, Brakenhoff RH, Takes RP. Novel diagnostic modalities for assessment of the clinically node-negative neck in oral squamous-cell carcinoma. *Lancet Oncol.* 2012;13:e554–61.
- Johnson DE, Burtness B, Leemans CR, Lui VVWY, Bauman JE, Grandis JR. Head and neck squamous cell carcinoma. *Nat Rev Dis Primers.* 2020;6:92.
- Chai AWY, Lim KP, Cheong SC. Translational genomics and recent advances in oral squamous cell carcinoma. *Semin Cancer Biol.* 2020;61:71–83.
- Pickering CR, Zhang J, Yoo SY, Bengtsson L, Moorthy S, Neskey DM, Zhao M, Ortega Alves MV, Chang K, Drummond J, et al. Integrative genomic characterization of oral squamous cell carcinoma identifies frequent somatic drivers. *Cancer Discov.* 2013;3:770–81.
- Marur S, D'Souza G, Westra WH, Forastiere AA. HPV-associated head and neck cancer: a virus-related cancer epidemic. *Lancet Oncol.* 2010;11:781–9.
- Pietrobon G, Tagliabue M, Stringa LM, De Berardinis R, Chu F, Zocchi J, Carlotto E, Chiocca S, Ansarin M. Leukoplakia in the oral cavity and oral microbiota: a comprehensive review. *Cancers (Basel).* 2021;13:4439.
- Zhong LP, Zhang CP, Ren GX, Guo W, William WN Jr, Sun J, Zhu HG, Tu WY, Li J, Cai YL, et al. Randomized phase III trial of induction chemotherapy with docetaxel, cisplatin, and fluorouracil followed by surgery versus up-front surgery in locally advanced resectable oral squamous cell carcinoma. *J Clin Oncol.* 2013;31:744–51.
- Civantos FJ, Zitsch RP, Schuller DE, Agrawal A, Smith RB, Nason R, Petruzelli G, Gourin CG, Wong RJ, Ferris RL, et al. Sentinel lymph node biopsy accurately stages the regional lymph nodes for T1–T2 oral squamous cell carcinomas: results of a prospective multi-institutional trial. *J Clin Oncol.* 2010;28:1395–400.
- Giacomello M, Pyakurel A, Glytsou C, Scorrano L. The cell biology of mitochondrial membrane dynamics. *Nat Rev Mol Cell Biol.* 2020;21:204–24.
- Narita T, Weinert BT, Choudhary C. Functions and mechanisms of non-histone protein acetylation. *Nat Rev Mol Cell Biol.* 2019;20:156–74.
- Zheng N, Shabek N. Ubiquitin ligases: structure, function, and regulation. *Annu Rev Biochem.* 2017;86:129–57.
- Rape M. Ubiquitylation at the crossroads of development and disease. *Nat Rev Mol Cell Biol.* 2018;19:59–70.
- Liu J, Qian C, Cao X. Post-translational modification control of innate immunity. *Immunity.* 2016;45:15–30.
- Tilokani L, Nagashima S, Paupe V, Prudent J. Mitochondrial dynamics: overview of molecular mechanisms. *Essays Biochem.* 2018;62:341–60.
- Zhang D, Tang Z, Huang H, Zhou G, Cui C, Weng Y, Liu W, Kim S, Lee S, Perez-Neut M, et al. Metabolic regulation of gene expression by histone lactylation. *Nature.* 2019;574:575–80.
- Moreno-Yruela C, Zhang D, Wei W, Bæk M, Liu W, Gao J, Danková D, Nielsen AL, Bolding JE, Yang L, et al. Class I histone deacetylases (HDAC1–3) are histone lysine delactylases. *Sci Adv.* 2022;8:eabi6696.
- Yang Z, Yan C, Ma J, Peng P, Ren X, Cai S, Shen X, Wu Y, Zhang S, Wang X, et al. Lactylome analysis suggests lactylation-dependent mechanisms of metabolic adaptation in hepatocellular carcinoma. *Nat Metab.* 2023;5:61–79.
- Hong H, Chen X, Wang H, Gu X, Yuan Y, Zhang Z. Global profiling of protein lysine lactylation and potential target modified protein analysis in hepatocellular carcinoma. *Proteomics.* 2023;23: e2200432.
- Yang D, Yin J, Shan L, Yi X, Zhang W, Ding Y. Identification of lysine-lactylated substrates in gastric cancer cells. *iScience.* 2022;25:104630.
- Wang L, Li S, Luo H, Lu Q, Yu S. PCSK9 promotes the progression and metastasis of colon cancer cells through regulation of EMT and PI3K/AKT signaling in tumor cells and phenotypic polarization of macrophages. *J Exp Clin Cancer Res.* 2022;41:303.
- Liu J, Du J, Li Y, Wang F, Song D, Lin J, Li B, Li L. Catalpol induces apoptosis in breast cancer in vitro and in vivo: involvement of mitochondria apoptosis pathway and post-translational modifications. *Toxicol Appl Pharmacol.* 2022;454:116215.
- Li X, Yang N, Wu Y, Wang X, Sun J, Liu L, Zhang F, Gong Y, Zhang Y, Li X, et al. Hypoxia regulates fibrosis-related genes via histone lactylation in the placentas of patients with preeclampsia. *J Hypertens.* 2022;40:1189–98.
- Yang J, Luo L, Zhao C, Li X, Wang Z, Zeng Z, Yang X, Zheng X, Jie H, Kang L, et al. A positive feedback loop between inactive VHL-triggered histone lactylation and PDGFR β signaling drives clear cell renal cell carcinoma progression. *Int J Biol Sci.* 2022;18:3470–83.
- Wang X, Fan W, Li N, Ma Y, Yao M, Wang G, He S, Li W, Tan J, Lu Q, et al. YY1 lactylation in microglia promotes angiogenesis through transcription activation-mediated upregulation of FGF2. *Genome Biol.* 2023;24:87.

25. Xiong J, He J, Zhu J, Pan J, Liao W, Ye H, Wang H, Song Y, Du Y, Cui B, et al. Lactylation-driven METTL3-mediated RNA m6A modification promotes immunosuppression of tumor-infiltrating myeloid cells. *Mol Cell*. 2022;82:1660–77.
26. Gu J, Zhou J, Chen Q, Xu X, Gao J, Li X, Shao Q, Zhou B, Zhou H, Wei S, et al. Tumor metabolite lactate promotes tumorigenesis by modulating MOESIN lactylation and enhancing TGF- β signaling in regulatory T cells. *Cell Rep*. 2022;39: 110986.
27. Fan M, Yang K, Wang X, Chen L, Gill PS, Ha T, Liu L, Lewis NH, Williams DL, Li C. Lactate promotes endothelial-to-mesenchymal transition via Snail1 lactylation after myocardial infarction. *Sci Adv*. 2023;9:eadc9465.
28. Wang J, Yang P, Yu T, Gao M, Liu D, Zhang J, Lu C, Chen X, Zhang X, Liu Y. Lactylation of pkm2 suppresses inflammatory metabolic adaptation in pro-inflammatory macrophages. *Int J Biol Sci*. 2022;18:6210–25.
29. Jing F, Zhang J, Cai X, Zhou X, Bai J, Zhang H, Li T. Screening for biomarkers for progression from oral leukoplakia to oral squamous cell carcinoma and evaluation of diagnostic efficacy by multiple machine learning algorithms. *Cancers (Basel)*. 2022;14:5808.
30. Tu HF, Chen MY, Lai JC, Chen YL, Wong YW, Yang CC, Chen HY, Hsia SM, Shih YH, Shieh TM. Arecoline-regulated ataxia telangiectasia mutated expression level in oral cancer progression. *Head Neck*. 2019;41:2525–37.
31. Wang YY, Wang WC, Su CW, Hsu CW, Yuan SS, Chen YK. Expression of Orai1 and STIM1 in human oral squamous cell carcinogenesis. *J Dent Sci*. 2022;17:78–88.
32. Hanahan D, Weinberg RA. Hallmarks of cancer: the next generation. *Cell*. 2011;144:646–74.
33. Hanahan D. Hallmarks of cancer: new dimensions. *Cancer Discov*. 2022;12:31–46.
34. Lyon RC, Cohen JS, Faustino PJ, Megnin F, Myers CE. Glucose metabolism in drug-sensitive and drug-resistant human breast cancer cells monitored by magnetic resonance spectroscopy. *Cancer Res*. 1988;48:870–7.
35. Nakashima RA, Paggi MG, Pedersen PL. Contributions of glycolysis and oxidative phosphorylation to adenosine 5'-triphosphate production in AS-30D hepatoma cells. *Cancer Res*. 1984;44:5702–6.
36. Fanciulli M, Bruno T, Giovannelli A, Gentile FP, Di Padova M, Rubiu O, Floridi A. Energy metabolism of human LoVo colon carcinoma cells: correlation to drug resistance and influence of lonidamine. *Clin Cancer Res*. 2000;6:1590–7.
37. Macheda ML, Rogers S, Best JD. Molecular and cellular regulation of glucose transporter (GLUT) proteins in cancer. *J Cell Physiol*. 2005;202:654–62.
38. Newsholme EA, Board M. Application of metabolic-control logic to fuel utilization and its significance in tumor cells. *Adv Enzyme Regul*. 1991;31:225–46.
39. Zhang L, Meng X, Zhu XW, Yang DC, Chen R, Jiang Y, Xu T. Long non-coding RNAs in Oral squamous cell carcinoma: biologic function, mechanisms and clinical implications. *Mol Cancer*. 2019;18:102.
40. Song X, Yang X, Narayanan R, Shankar V, Ethiraj S, Wang X, Duan N, Ni YH, Hu Q, Zare RN. Oral squamous cell carcinoma diagnosed from saliva metabolic profiling. *Proc Natl Acad Sci U S A*. 2020;117:16167–73.
41. Liu X, He Y, Li F, Huang Q, Kato TA, Hall RP, Li CY. Caspase-3 promotes genetic instability and carcinogenesis. *Mol Cell*. 2015;58:284–96.
42. Vaishnavi A, Scherzer MT, Kinsey CG, Parkman GL, Truong A, Ghazi P, Schuman S, Battistone B, Garrido-Laguna I, McMahon M. Inhibition of MEK1/2 forestalls the onset of acquired resistance to entrectinib in multiple models of NTRK1-driven cancer. *Cell Rep*. 2020;32: 107994.
43. Jain A, Bacolla A, Del Mundo IM, Zhao J, Wang G, Vasquez KM. DHX9 helicase is involved in preventing genomic instability induced by alternatively structured DNA in human cells. *Nucleic Acids Res*. 2013;41:10345–57.
44. Liu L, Zhou X, Cheng S, Ge Y, Chen B, Shi J, Li H, Li S, Li Y, Yuan J, et al. RNA-binding protein DHX9 promotes glioma growth and tumor-associated macrophages infiltration via TCF12. *CNS Neurosci Ther*. 2023;29:988–99.
45. Liu MY, Lin KR, Chien YL, Yang BZ, Tsui LY, Chu HC, Wu CP. ATR phosphorylates DHX9 at serine 321 to suppress R-loop accumulation upon genotoxic stress. *Nucleic Acids Res*. 2024;52:204–22.
46. Chakraborty P, Hiom K. DHX9-dependent recruitment of BRCA1 to RNA promotes DNA end resection in homologous recombination. *Nat Commun*. 2021;12:4126.
47. Chakraborty P, Huang J TJ, Hiom K. DHX9 helicase promotes R-loop formation in cells with impaired RNA splicing. *Nat Commun*. 2018;9:4346.
48. Parker DM, Bublitz GR, Parker R. Shining light on DHX9: UV-induced stress granules illuminate protective mechanisms for daughter cell resilience. *Mol Cell*. 2024;84:1403–5.
49. Murayama T, Nakayama J, Jiang X, Miyata K, Morris AD, Cai KQ, Prasad RM, Ma X, Efimov A, Belani N, et al. Targeting DHX9 triggers tumor-intrinsic interferon response and replication stress in small cell lung cancer. *Cancer Discov*. 2024;14:468–91.
50. Semenza GL. Targeting HIF-1 for cancer therapy. *Nat Rev Cancer*. 2003;3:721–32.
51. Choudhry H, Harris AL. Advances in hypoxia-inducible factor biology. *Cell Metab*. 2018;27:281–98.
52. Wang J, Jiang C, Li N, Wang F, Xu Y, Shen Z, Yang L, Li Z, He C. The circEPST11/mir-942-5p/LTBP2 axis regulates the progression of OSCC in the background of OSF via EMT and the PI3K/Akt/mTOR pathway. *Cell Death Dis*. 2020;11:682.
53. Ma S, Meng Z, Chen R, Guan KL. The Hippo pathway: biology and pathophysiology. *Annu Rev Biochem*. 2019;88:577–604.
54. Cunningham R, Hansen CG. The Hippo pathway in cancer: YAP/TAZ and TEAD as therapeutic targets in cancer. *Clin Sci (Lond)*. 2022;136:197–222.
55. Zhu N, Yang R, Wang X, Yuan L, Li X, Wei F, Zhang L. The Hippo signaling pathway: from multiple signals to the hallmarks of cancers. *Acta Biochim Biophys Sin (Shanghai)*. 2023;55:904–13.
56. Huang N, Song Y, Shi W, Guo J, Zhang Z, He Q, Wu L, Li X, Xu F. DHX9-mediated pathway contributes to the malignant phenotype of myelodysplastic syndromes. *iScience*. 2023;26:106962.
57. Chellini L, Scarfò M, Bonvissuto D, Sette C, Paronetto MP. The DNA/RNA helicase DHX9 orchestrates the KDM2B-mediated transcriptional regulation of YAP1 in Ewing sarcoma. *Oncogene*. 2024;43:225–34.
58. Wang Y, Guo Y, Song Y, Zou W, Zhang J, Yi Q, Xiao Y, Peng J, Li Y, Yao L. A pan-cancer analysis of the expression and molecular mechanism of DHX9 in human cancers. *Front Pharmacol*. 2023;14:1153067.
59. Liu S, He L, Wu J, Wu X, Xie L, Dai W, Chen L, Xie F, Liu Z. DHX9 contributes to the malignant phenotypes of colorectal cancer via activating NF- κ B signaling pathway. *Cell Mol Life Sci*. 2021;78:8261–81.

60. Zhang Q, Meng F, Chen S, Plouffe SW, Wu S, Liu S, Li X, Zhou R, Wang J, Zhao B, et al. Hippo signalling governs cytosolic nucleic acid sensing through YAP/TAZ-mediated TBK1 blockade. *Nat Cell Biol.* 2017;19:362–74.
61. Fu M, Hu Y, Lan T, Guan KL, Luo T, Luo M. The Hippo signalling pathway and its implications in human health and diseases. *Signal Transduct Target Ther.* 2022;7:376.
62. Whitcomb DC, Lowe ME. Human pancreatic digestive enzymes. *Dig Dis Sci.* 2007;52:1–17.
63. Tyanova S, Temu T, Cox J. The MaxQuant computational platform for mass spectrometry-based shotgun proteomics. *Nat Protoc.* 2016;11:2301–19.
64. Buenostro JD, Giresi PG, Zaba LC, Chang HY, Greenleaf WJ. Transposition of native chromatin for fast and sensitive epigenomic profiling of open chromatin, DNA-binding proteins and nucleosome position. *Nat Methods.* 2013;10:1213–8.
65. Kaya-Okur HS, Wu SJ, Codomo CA, Pledger ES, Bryson TD, Henikoff JG, Ahmad K, Henikoff S. CUT&Tag for efficient epigenomic profiling of small samples and single cells. *Nat Commun.* 2019;10:1930.
66. Barbie DA, Tamayo P, Boehm JS, Kim SY, Moody SE, Dunn IF, Schinzel AC, Sandy P, Meylan E, Scholl C, et al. Systematic RNA interference reveals that oncogenic KRAS-driven cancers require TBK1. *Nature.* 2009;462:108–12.
67. Liberzon A, Birger C, Thorvaldsdóttir H, Ghandi M, Mesirov JP, Tamayo P. The Molecular Signatures Database (MSigDB) hallmark gene set collection. *Cell Syst.* 2015;1:417–25.
68. Perez-Riverol Y, Bai J, Bandla C, García-Seisdedos D, Hewapathirana S, Kamatchinathan S, Kundu DJ, Prakash A, Frericks-Zipper A, Eisenacher M, et al. The PRIDE database resources in 2022: a hub for mass spectrometry-based proteomics evidences. *Nucleic Acids Res.* 2022;50:D543–52.
69. Jing F, Zhu L, Zhang J, Zhou X, Bai J, Li X, Zhang H, Li T. Multi-omics reveals lactylation-driven regulatory mechanisms promoting tumor progression in oral squamous cell carcinoma. Datasets. ProteomeXchange Consortium repositories. <https://www.ebi.ac.uk/pride/archive/projects/PXD047535>. 2024.
70. Jing F, Zhu L, Zhang J, Zhou X, Bai J, Li X, Zhang H, Li T. Multi-omics reveals lactylation-driven regulatory mechanisms promoting tumor progression in oral squamous cell carcinoma. Datasets. ProteomeXchange Consortium repositories. <https://www.ebi.ac.uk/pride/archive/projects/PXD047673>. 2024.
71. Jing F, Zhu L, Zhang J, Zhou X, Bai J, Li X, Zhang H, Li T. Multi-omics reveals lactylation-driven regulatory mechanisms promoting tumor progression in oral squamous cell carcinoma. Datasets. Gene Expression Omnibus (GEO). <https://www.ncbi.nlm.nih.gov/geo/query/acc.cgi?acc=GSE249223>. 2024.
72. Jing F, Zhu L, Zhang J, Zhou X, Bai J, Li X, Zhang H, Li T. Multi-omics reveals lactylation-driven regulatory mechanisms promoting tumor progression in oral squamous cell carcinoma. Datasets. Gene Expression Omnibus (GEO). <https://www.ncbi.nlm.nih.gov/geo/query/acc.cgi?acc=GSE249224>. 2024.
73. Jing F, Zhu L, Zhang J, Zhou X, Bai J, Li X, Zhang H, Li T. Multi-omics reveals lactylation-driven regulatory mechanisms promoting tumor progression in oral squamous cell carcinoma. Datasets. Gene Expression Omnibus (GEO). <https://www.ncbi.nlm.nih.gov/geo/query/acc.cgi?acc=GSE249226>. 2024.

Publisher's Note

Springer Nature remains neutral with regard to jurisdictional claims in published maps and institutional affiliations.